View metadata, citation and similar papers at core.ac.uk
brought to you by CORE
provided by Elsevier - Publisher Connector

Biophysical Journal Volume 96 May 2009 3519–3528

Peptide Nanopores and Lipid Bilayers: Interactions by Coarse-Grained Molecular-Dynamics Simulations

Jochen W. Klingelhoefer, Timothy Carpenter, and Mark S. P. Sansom*
Department of Biochemistry, University of Oxford, Oxford, United Kingdom

ABSTRACT A set of 49 protein nanopore-lipid bilayer systems was explored by means of coarse-grained molecular-dynamics simulations to study the interactions between nanopores and the lipid bilayers in which they are embedded. The seven nanopore species investigated represent the two main structural classes of membrane proteins (α-helical and β-barrel), and the seven different bilayer systems range in thickness from ~28 to ~43 Å. The study focuses on the local effects of hydrophobic mismatch between the nanopore and the lipid bilayer. The effects of nanopore insertion on lipid bilayer thickness, the dependence between hydrophobic thickness and the observed nanopore tilt angle, and the local distribution of lipid types around a nanopore in mixed-lipid bilayers are all analyzed. Different behavior for nanopores of similar hydrophobic length but different geometry is observed. The local lipid bilayer perturbation caused by the inserted nanopores suggests possible mechanisms for both lipid bilayer-induced protein sorting and protein-induced lipid sorting. A correlation between smaller lipid bilayer thickness (larger hydrophobic mismatch) and larger nanopore tilt angle is observed and, in the case of larger hydrophobic mismatches, the simulated tilt angle distribution seems to broaden. Furthermore, both nanopore size and key residue types (e.g., tryptophan) seem to influence the level of protein tilt, emphasizing the reciprocal nature of nanopore-lipid bilayer interactions.

INTRODUCTION

Membranes play a key role in the biology of cells and in a number of nanotechnological applications. Cell membranes consist of lipid bilayers plus a wide range of membrane proteins, including pores, channels, and transporters. A measure of the importance of membrane proteins is provided by the observation that they account for ~25% of all genes. Furthermore, despite initially slow progress, determination of membrane protein structures is growing exponentially.

It is evident that studies of the function of membrane proteins must take into account the interactions of these proteins with their lipid bilayer environment. In particular, the hydrophobic thickness and composition of lipid bilayers have been shown to influence the biological activity of membrane proteins (1). Unfortunately, crystal structures rarely contain explicit information on where the proteins are located in the bilayer. Computational approaches provide one way in which to complement the available experimental data (2).

A number of experimental and computational studies on protein-membrane interactions have focused on simplified model systems such as single transmembrane (TM) α-helices (3–6) or simplified models of proteins or nanopores (7–10). The latter are simple models of TM pores that span lipid bilayers and have diameters in the range of ~1–5 Å. There is a need to extend beyond simple models to a wider range of more biologically representative models of transbilayer pores and their interactions with lipid bilayers. In particular, given the importance of pores in biology and in nanoscience (11), we focus here on a systematic exploration of various polypeptide nanopores and their interactions with lipid bilayers.

There has been considerable success in the use of molecular-dynamics (MD) simulations to study membranes (2). Such simulations complement experimental studies of membranes and their proteins (12). An additional strength of MD and related simulations is that they enable the exploration of local perturbations of the lipid bilayer in the vicinity of the proteins (13–16), which may otherwise be difficult to study.

To overcome some of the limits on complexity and simulation time presented by atomistic MD (AT-MD) simulations of nanopore-lipid bilayer systems, a coarse-grained MD (CG-MD) approach may be employed. In the CG-MD approach (12,15,17–30), small groups of atoms are treated as single particles, reducing system complexity and thus allowing for longer timescales and larger systems to be simulated. For example, in our approach (which is based on a CG-MD system proposed by Marrink and colleagues (12,27,31)), groups of ~4 nonhydrogen atoms are clustered together and represented by one CG particle. The main benefit of CG-MD methods is the aforementioned significant reduction in system complexity, resulting in a reduction of simulation time by two to three orders of magnitude. This extends the complexity and duration of simulation studies of these systems, thus enabling better sampling. The CG-MD approach based on the work of Marrink and colleagues was recently employed for a number of simulation studies of biological ion channels (32).

A central concept of protein-lipid bilayer systems is referred to as ''hydrophobic mismatch'' (33), which describes the differences in length between the hydrophobic

Submitted November 11, 2008, and accepted for publication January 13, 2009.

*Correspondence: mark.sansom@bioch.ox.ac.uk

Editor: Gregory A. Voth.

© 2009 by the Biophysical Society

0006-3495/09/05/3519/10 $2.00

doi: 10.1016/j.bpj.2009.01.046

TABLE 1 Sequences of model nanopores

Nanopore	Sequence* of monomer†
M2: M2δ TM domain	EK**M**ST**AI**S**VLLA**Q**AVFLLL**TSQR
Gα: generalized α-helix bundle (with Trp residues)	S<u>W</u>**L**SS**LL**S**LL**SS**LL**S**LL**SS<u>W</u>**L**S**L**
Nα: generalized α-helix bundle (without Trp residues)	S**LL**SS**LL**S**LL**SS**LL**S**LL**SS**LL**S**L**
HL: α-hemolysin TM domain	TKEY**M**ST**L**TYG**F**NGN**V**TGDDTGK**I**GG**LI**G**A**NVS**I**GHT**L**KYVQP
Gβ: generalized β-barrel (with Trp residues)	S**L**S**L**S**L**S**L**S**L**S**L**S**L**S<u>W</u>S**L**S**L**S**L**S**L**S**L**S**L**S**L**S<u>W</u>S**L**S
Nβ: generalized β-barrel (without Trp residues)	S**L**S**L**S**L**S**L**S**L**S**L**S**L**S**L**S**L**S**L**S**L**S**L**S**L**S**L**S**L**S**L**S
Sβ: short β-barrel	S**L**S**L**S**L**S**L**S**L**S<u>W</u>S**L**S**L**S**L**S**L**S**L**S**L**S<u>W</u>S**L**S

*Hydrophobic residues are in bold font, and Trp residues are underlined.
†For the β-barrels the monomer corresponds to a β-hairpin; thus, seven monomers make up the 14-strand β-barrel. For the α-helix bundles the monomer corresponds to an individual α-helix, five of which constitute the bundle.

regions of the protein and the lipid bilayer. This mismatch, together with the surface structure of a protein nanopore, is thought to be mainly responsible for local bilayer deformation (34), given that lipid bilayers are more easily deformed than protein. Therefore, the bilayer locally deforms to try to match the hydrophobic region of the protein, minimizing the local perturbations introduced by the protein (35).

The hydrophobic mismatch between a protein nanopore and the surrounding lipid bilayer may show one of three distinct characteristics:

1. If the hydrophobic length of the nanopore is significantly longer than the hydrophobic length of the lipid bilayer, the nanopore will induce local bilayer stretching.
2. If the hydrophobic length of the nanopore is significantly shorter than the hydrophobic length of the lipid bilayer, the nanopore will induce local bilayer compression.
3. If the hydrophobic length of the nanopore and the lipid bilayer approximately match, the lipid bilayer will not experience any noticeable local perturbation.

If the hydrophobic mismatch exceeds a certain level, the local bilayer deformation alone will not be sufficient to compensate for the degree of mismatch, resulting in either tilting of the nanopore relative to the bilayer normal and/or distortion of the protein.

In this study we used CG-MD to systematically study a set of 49 nanopore-lipid bilayer systems (i.e., 7 nanopores $\times$ 7 lipid bilayer systems) to probe interactions occurring over a range of parameters, e.g., membrane protein class, lipid species, and bilayer thickness. The nanopores studied in this work are representative of the two generic classes of TM proteins: α-helical bundles and β-barrels. The majority of TM proteins are α-helical (36), whereas β-barrel TM proteins are found primarily in the outer membranes of Gram-negative bacteria and in some secreted membrane-active bacterial toxins.

The results of this study provide a systematic approach to examine the mutual interactions between lipid bilayers and protein nanopores. As such, they significantly extend studies of single-membrane proteins and/or simplified nanopore/membrane protein systems (8–10,12,14,16,20,25,37). In particular, we extend previous studies by systematically exploring a range of pore models (both α-helix bundles and β-barrels), focusing on the role of some key membrane-interacting residues, such as Trp.

MATERIALS AND METHODS

Nanopore models

In this study we focused on seven model pores (Table 1, Fig. 1). The first two nanopore studies were the nicotinic receptor M2δ helical bundle

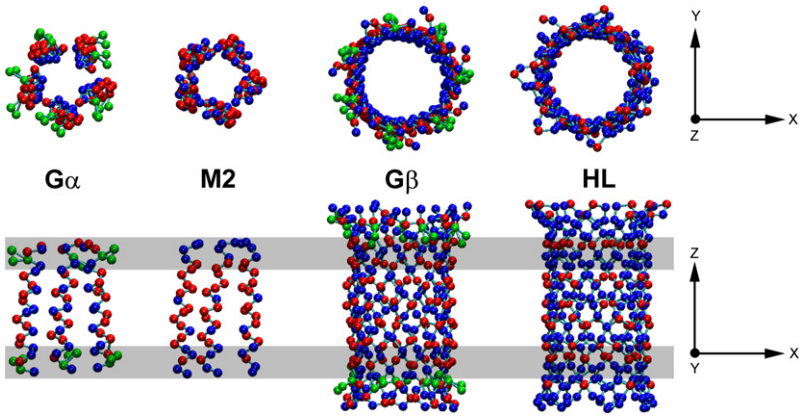

FIGURE 1 CG structures of the nanopores employed in this study viewed down the bilayer normal (*z*; *upper row*) and perpendicular to the bilayer normal (*lower row*). The generalized α-helical nanopore (Gα), nicotinic receptor M2 TM domain (M2), generalized β-barrel nanopore (Gβ), and α-hemolysin TM domain (HL) are shown. (The second set of generalized nanopores, in which the Trp residues were replaced by Leu residues (Nα, Nβ), as well as the shortened, generalized β-barrel nanopore (Sβ), where the TM region has been capped by two residues rings, are not depicted.) Hydrophobic (mostly outer surface of the nanopores), hydrophilic (mostly inner surface of nanopores), and (where present) membrane-anchoring Trp residues (residue rings around the nanopore ends) are highlighted. Also sketched is the approximate position of each nanopore within a lipid bilayer, with the headgroups of the two bilayer leaflets indicated as gray bands. The lipid bilayers lie in the *x*-*y* plane, and the bilayer normal and central axes of the nanopores are oriented in the *z* direction.

(M2; PDB ID: 1EQ8) (38), a simple α-helical nanopore (39), and the TM domain of Staphylococcal α-hemolysin (HL; PDB ID: 7AHL), a β-barrel nanopore of technological importance (40). These are representative of the two classes of protein nanopore structure: an α-helix bundle and a β-barrel. Each of these two nanopores was also simplified to yield four generalized nanopore structures: Gα, Gβ, Nα, and Nβ, respectively. Note that Gα and Gβ each featured TM domains with a hydrophobic outer surface, composed of leucine (Leu, L) residues, a hydrophilic interior pore lining, composed of serine (Ser, S) residues, and two rings (one at each end of the nanopore) of membrane-anchoring tryptophan (Trp, W) residues (41,42). Nα and Nβ are identical to Gα and Gβ, with the exception that they have Leu residues in place of Trp residues. These four nanopores enabled us to study interactions between nanopore residues and phospholipid headgroups, as well as the impact of Trp on these interactions. A further β-barrel nanopore, Sβ, was generated by shortening the TM domain of the generalized β-barrel Gβ by two rings of residues to make its bilayer-spanning region more comparable in hydrophobic length to the generalized α-helical nanopore Gα. Note that the sequence and proposed structure of the Gα nanopore resemble those of the de novo designed peptide pore of Lear et al. (43).

Preparation of the nanopore-bilayer systems

We used a range of CG lipid species, each consisting of a phosphatidylcholine (PC) headgroup with between two (CG2-PC) and five (CG5-PC) hydrophobic CG particles per fatty acyl chain. The approximate correspondences between the CG lipid models and the corresponding atomistic lipid species are as follows: 1), CG2-PC $\approx$ dioctanoyl PC, $(C8:0)_2$PC; 2), CG3-PC $\approx$ dilauroyl PC, $(C12:0)_2$PC; 3), CG4-PC $\approx$ dipalmitoyl PC, $(C16:0)_2$; and 4), CG5-PC $\approx$ dieicosanoyl PC, $(C20:0)_2$PC. Bilayers of intermediate thickness were generated by mixtures (all 1:1) of 1), CG2-PC + CG3-PC; 2), CG3-PC + CG4-PC; and 3), CG4-PC + CG5-PC. Together, the seven different lipid bilayer systems and seven nanopore models formed a set of 49 systems, enabling detailed comparative analyses. Note that CG3-PC, CG4-PC, and CG5-PC were studied previously by Periole and colleagues (16).

Membrane self-assembly simulations (44,45) were performed to establish a library of seven preformed lipid bilayer systems (in order of increasing bilayer thickness): CG2-PC, CG2-PC + CG3-PC, CG3-PC, CG3-PC + CG4-PC, CG4-PC, CG4-PC + CG5-PC, and CG5-PC. These systems were energy minimized (using the steepest-descent method in GROMACS; see below) and the bilayers were centered with the bilayer normal in the z direction. Next, all nanopores were energy minimized and then inserted into the bilayer centers, as sketched in Fig. 1.

After a subsequent energy-minimization step, the systems were solvated with CG water particles and when necessary neutralized with CG counterions. Another energy minimization was run to relax any steric conflicts. Finally, a production simulation of 200 ns was run for all 49 systems. The composition and size of all resultant nanopore-lipid bilayer systems can be found in the Supporting Material (Fig. S1, Table S1).

Simulation details

For the CG-MD simulations, the GROMACS simulation package (46) (available at www.gromacs.org) was employed. The CG representations of the nanopore residues, phospholipids, water molecules, and salt ions were chosen according to a modified version of the Marrink model (12,26,27,45) in which each CG particle represents ~4 nonhydrogen atoms. An elastic network model was used to represent protein secondary and tertiary structure (26) with a force constant of 1000 kJ mol^{-1} nm^{-2} and cutoff distances of 1 nm and 0.7 nm for α-helical and β-barrel nanopores, respectively. The larger cutoff distance for α-helical nanopores was necessary because their structures contain only contacts on one side of the pore, resulting in a compression of the pore when inserted into the lipid bilayer. As we were interested in how interactions with the lipid bilayer are influenced by the different outer surfaces of nanopores of the two classes, such a choice of parameters seems legitimate. Further details of the CG force field may be found in previous publications (26,45,47,48).

In the MD simulations the time step for integration was 40 fs and simulation frames were stored every 400 ps for subsequent analysis. The nonbonded neighbor list was updated every 10 steps and all simulations were performed at constant number of particles, pressure, and temperature (NPT ensemble). The temperatures of the protein, lipids, and solvent were each coupled separately using the Berendsen algorithm (49) at 323 K with a coupling constant of 10 ps. The system pressure was isotropically coupled (12) using the Berendsen algorithm at 1 bar with a coupling constant of 10 ps and a compressibility of 5×10^{-6} bar^{-1}. The effects of switching to semi-isotropic pressure coupling were investigated and resulted in qualitatively similar findings with slightly larger bilayer thickness. All the essential effects, such bilayer perturbation and protein tilt angle versus hydrophobic thickness traces, were preserved. A comparison can be found in the Supporting Material.

All analyses were performed using GROMACS tools, MATLAB (The MathWorks, Natick, MA), and local shell and Perl scripts. VMD (50) was used for visualization.

RESULTS

Lipid bilayer parameters

Before analyzing the impact of polypeptide nanopores on the various lipids bilayers, we wished to characterize the bilayers on their own. Thus, various parameters were calculated for the single-lipid type (CG2-PC, CG3-PC, CG4-PC, CG5-PC) and mixed-lipid type (CG2-PC+CG3-PC, CG3-PC+CG-4PC, CG4-PC+CG5-PC) bilayer systems and compared with available experimental and atomistic simulation data. Reasonable agreement was obtained (data not shown; see Marrink et al. (12)). Of particular relevance to the current study is the bilayer thickness (defined as the distance between the phosphate particles of opposing monolayers), which is presented in the Supporting Material (Fig. S1) for the various systems employed in our study.

Because in our chosen CG-MD method ~4 carbon atoms are grouped together to form the CG carbon particles of the lipid tails, the simulated lipid bilayer thickness will not exactly match the corresponding experimental values. For example, for CG4-PC the current simulations yield a thickness of 39 Å, compared with values for DPPC of 37 Å for experiment (cited in Tieleman and Berendsen (51)) and a range of 35–37 Å in atomistic simulations (51).

Bilayer perturbation introduced by nanopore insertion

To study the perturbations introduced by the insertion of nanopores into lipid bilayers, the 49 systems were set up as described and simulated for 200 ns (except for the systems displayed in Fig. 2, which were simulated for 500 ns to improve sampling and hence reduce noise). The resulting particle trajectories were analyzed according to the procedures outlined in the Materials and Methods section. Fig. 2 summarizes the results for the lipid bilayer perturbations for the generalized α-helical (Gα) and shortened β-barrel (Sβ) nanopores. For the Gα systems, the transition from local bilayer stretching (in the CG2-PC lipid bilayer) to local bilayer compression (in the CG5-PC lipid bilayer) can be

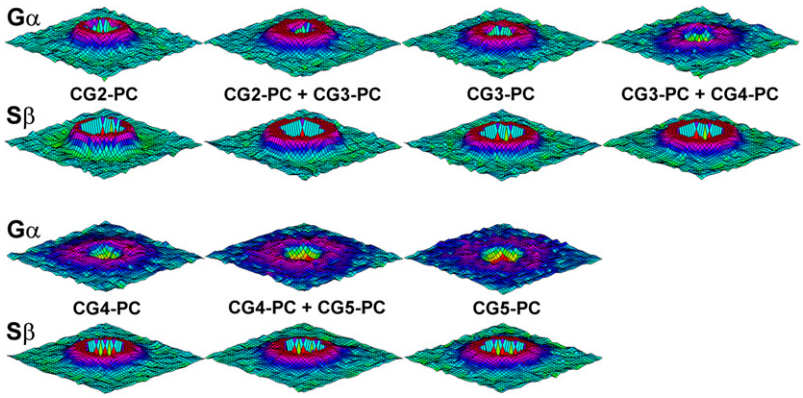

FIGURE 2 Time-averaged lipid bilayer perturbation introduced by the insertion of a generalized α-helical nanopore (Gα) and a shortened β-barrel nanopore (Sβ) into various lipid bilayers for 500 ns CG-MD simulations. The relative variation of the lipid bilayer from the unperturbed bilayer mean is displayed. For clarity, nanopores are not displayed, and the bilayer thickness profiles for the Sβ nanopore systems are displayed in the z direction with an applied cutoff of 3 Å from the bilayer COM.

seen. The Sβ nanopore systems show the lipid bilayer locally stretched for all bilayer systems, originating in the fact that the hydrophobic length of the nanopore is always larger than the hydrophobic length of the lipid bilayer. Furthermore, the Sβ nanopore-CG2-PC lipid bilayer system shows the presence of an undershoot, which can be explained by lipids in that region having to satisfy both the matching constraints with the nanopore and the constant density constraint for the overall lipid bilayer system (9).

Radial lipid bilayer perturbation profiles for all nanopores studied are displayed in Figs. 3 and 4. For the α-helical nanopores (Fig. 3), the transition from local bilayer stretching to local bilayer compression can be seen for the M2 helical bundle, the Gα nanopore, and the Nα nanopore. Thus, when the lipid bilayer thickness is varied from the thinnest (CG2-PC) to the thickest (CG5-PC) system, for all α-helical systems, a transition from local bilayer stretching (the hydrophobic length of the nanopore is longer than the hydrophobic length of the lipid bilayer; lipids stretch and become more gel-like) through the ''neutral'' state (the hydrophobic lengths of the nanopore and lipid bilayer match) to local bilayer compression (the hydrophobic length of the nanopore is shorter than the hydrophobic length of the lipid bilayer; lipids compress) is observed. The first derivatives of the radial bilayer thickness profiles show that the local bilayer perturbations, caused by the inserted nanopore, subside at a distance of ~40 Å from the nanopore center of mass (COM) for all systems (in broad agreement with earlier studies of simplified model proteins (9)). Of interest, although they are comparable in terms of hydrophobic thickness (cf. Supporting Material, Fig. S2, Fig. S3, Table S2), M2, Gα, and Nα differ in the details of their radial bilayer thickness profiles. The Gα and Nα profiles show a greater complexity and much more distinct transition from stretching to compression than the M2 profiles, with much less of a difference between the Gα and Nα profiles. Therefore, it seems that the modification of the residues of M2 to generate a purely hydrophobic outer surface plus a purely hydrophilic interior (pore) surface has a much stronger effect than the inclusion/exclusion of Trp residues, even though a small effect of the latter may be observed.

Turning to the β-barrel nanopores, both HL and the Sβ nanopore show similar radial bilayer thickness profiles, whereas the Gβ nanopore forces the bilayer into considerable local stretching due to the more pronounced hydrophobic mismatch. For HL and Sβ in the thicker bilayer systems (CG4-PC+CG5-PC and CG5-PC), the local perturbations approach a neutral state (matched hydrophobic lengths between the nanopore and lipid bilayer). This is in contrast to the Gβ systems, where, due to a much larger degree of

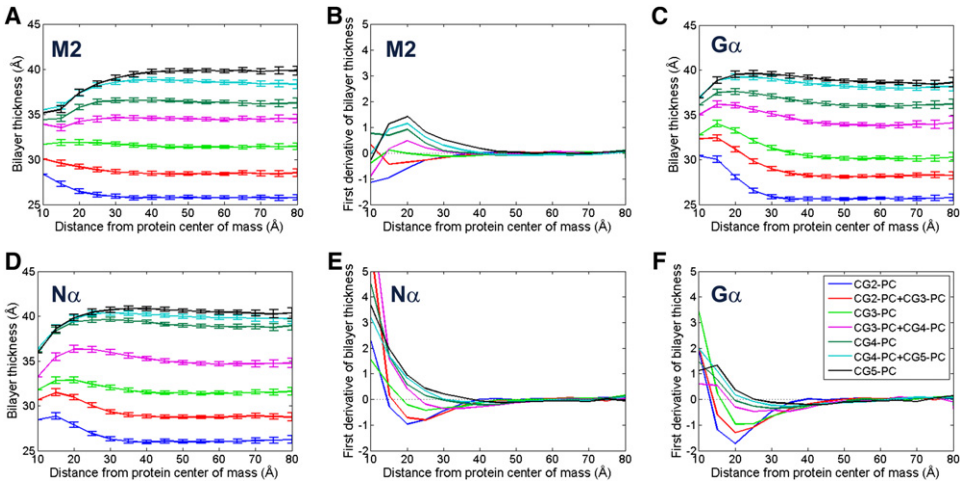

FIGURE 3 Radial bilayer thickness profiles and first derivatives for the M2 helical bundle (*A* and *B*), the Gα nanopore (*C* and *F*), and the Nα nanopore (*D* and *E*) simulations. The radial distance is measured from the nanopore COM. (For clarity, the displayed standard deviation (SD) has been scaled by a factor of 0.25.)

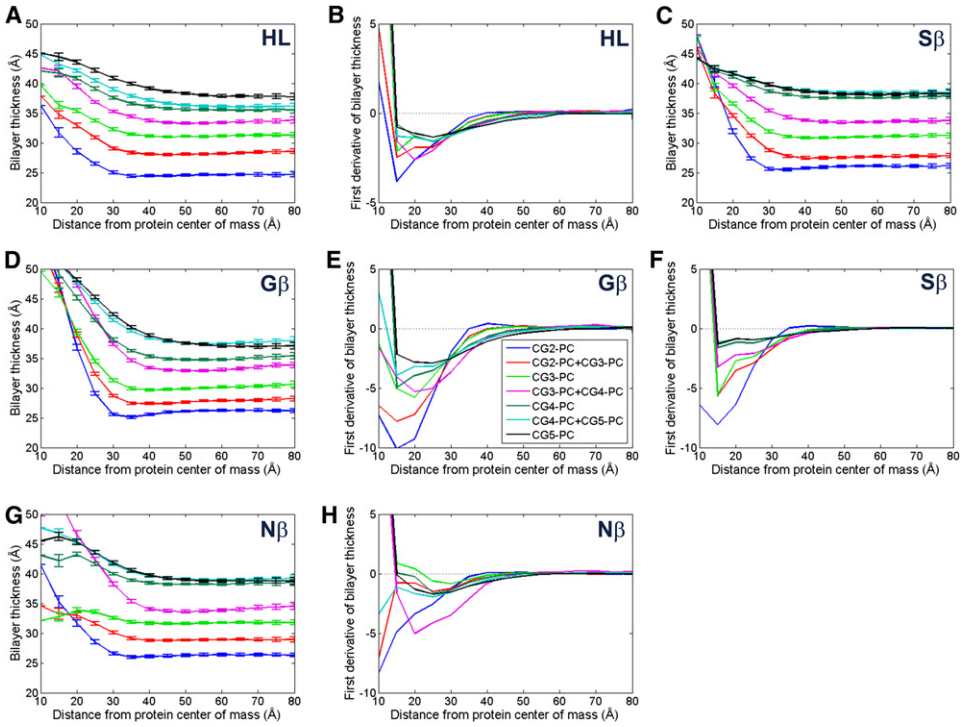

FIGURE 4 Radial bilayer thickness profiles and first derivatives for the α-hemolysin (HL) transbilayer pore (*A* and *B*), the Gβ nanopore (*D* and *E*), the Nβ nanopore (*G* and *H*), and the Sβ nanopore (*C* and *F*) simulations. The radial distance is measured from the nanopore COM. (For clarity, the displayed SD has been scaled by a factor of 0.25.)

hydrophobic mismatch (cf. Supporting Material, Fig. S2, Fig. S3), the lipid bilayer remains locally stretched for all lipid systems studied. The Nβ systems show a much less consistent behavior, which resembles that of the HL systems more closely than that of the generalized (Gβ) systems. This indicates that, in contrast to α-helical systems, in the β-barrel systems the Trp residues appear to be more important for aligning the pore in the lipid bilayer. In addition to the degree of hydrophobic mismatch, the extent of the perturbations also seems to depend on the nanopore length, as suggested by previous studies (52).

The first derivatives of the radial bilayer thickness profiles clarify that the local bilayer perturbations, caused by the insertion of the nanopores, approximately follow an exponential law and decay in a distance of 30–60 Å from the nanopore COM, which is in good agreement with previous findings from dissipative particle dynamics simulations of simple models of proteins (9). Thus, for example, for HL the first derivative returns to zero at ~40 Å from the nanopore center for the CG2-PC bilayer, but not until ~60 Å from the nanopore for the CG5-PC bilayer.

The undershoot present in the lipid bilayer thickness profiles between 30 and 50 Å away from the nanopore for β-barrel nanopores embedded in CG2-PC lipid bilayers (Fig. 4) can be explained by the fact that lipids in that region have to satisfy both the matching constraints with the nanopore and the constant density constraint for the overall lipid bilayer system (9). As a consequence, lipids near the nanopore surface change their length to match the hydrophobic length of the nanopore, whereas their neighboring lipids tilt toward (undershooting) or away from (overshooting) the nanopore to satisfy the constant density constraint, locally thinning or thickening the lipid bilayer, respectively.

When we compare the values of the undisturbed phosphate-phosphate thickness for all lipid bilayers (cf. Supporting Material, Fig. S1) with the results described in this section, it is evident that the lipid bilayers in these systems relax to an equilibrium value that is slightly smaller than the one calculated for undisturbed lipid bilayer systems. This may reflect periodicity effects due to the box size of these systems (chosen to optimize the computation time for the 49 systems). To evaluate the magnitude of this effect, a number of systems were simulated with a fourfold-larger area bilayer. The results show that the lipid bilayers in these larger systems relaxed to an equilibrium value that matched those of the undisturbed lipid bilayer systems (cf. Supporting Material, Fig. S11).

Lipid bilayer-introduced nanopore tilt

There is a considerable body of experimental (5,6,53,54) and computational (55,56) data concerning protein/lipid bilayer mismatch and protein tilting relative to the bilayer for single TM helix model systems. It is therefore of interest to extend such analyses to more complex protein nanopores.

A simple visual comparison of the degree of tilting for the various simulations (Fig. 5) performed suggests that a mismatch between the nanopore as a whole and the bilayer thickness mainly determines the degree of tilt. Thus, for example, the Gα nanopore shows only a relatively small degree of tilt, regardless of the thickness of the bilayer. In contrast, the Gβ bundle (for which the degree of mismatch

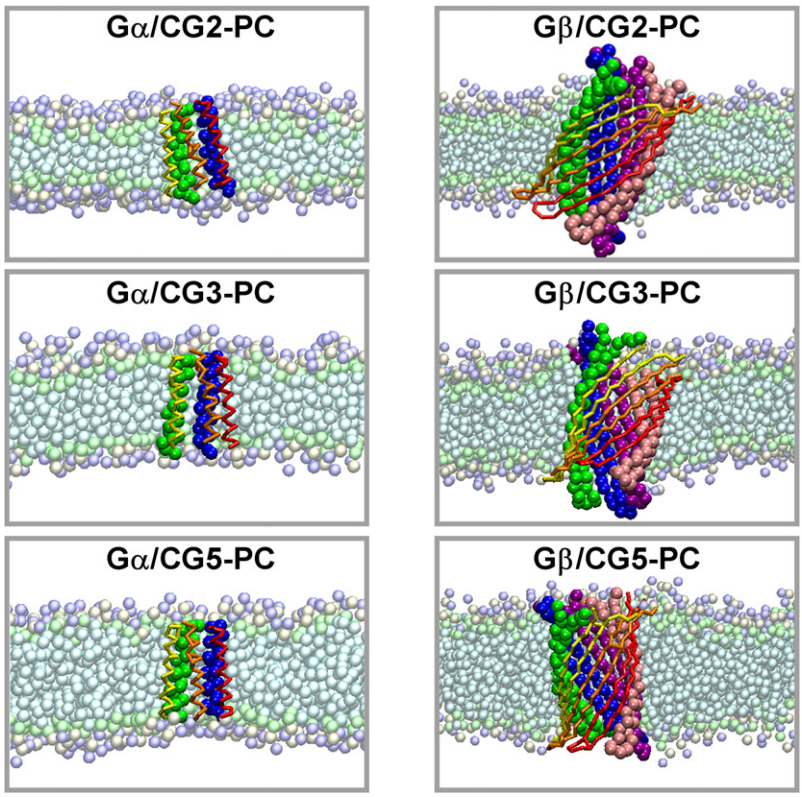

FIGURE 5 Tilt of nanopores as a function of nanopore model (Gβ versus Gα) and bilayer thickness (CG2 versus CG3 versus CG5PC). Snapshots from the simulations are shown. Nanopore secondary structure elements are highlighted and the bilayer is depicted in darker and lighter shades for lipid headgroups and hydrophobic tails, respectively.

is greater) exhibits a strong dependency of the degree of tilt upon the bilayer thickness (i.e., the lipid species involved).

To quantify the nanopore tilt angle relative to the bilayer, the upper and lower rings of residues were defined for each nanopore and the COM of each ring was computed. Next, the average angle between a vector spanned by the two COMs and the bilayer normal vector (z axis) was computed for each simulation. The results of this analysis, in terms of mean tilt angles for all 49 systems, are shown in Fig. 6 and values for the maximum tilt angles can be found in the Supporting Material (Fig. S7).

From this analysis it is evident that a correlation exists between a smaller lipid bilayer thickness (i.e., a larger hydrophobic mismatch) and larger tilt angle occurring for both classes of nanopores. Also, in the case of larger hydrophobic mismatch, the tilt angle distribution broadens (cf. Supporting Material, Fig. S8), indicating a more substantial tilting fluctuation of nanopores in these systems. When the different nanopores are compared, all systems seem to follow this trend. Thus, the mean tilt angles present in the nanopore-lipid bilayer systems increase in the following order: M2, Gα, Nα, Sβ, HL, Nβ, and Gβ. Of interest, even though HL, Nβ, and Gβ have comparable hydrophobic lengths (cf. Supporting Material), the tilt angle is higher for Nβ and Gβ, possibly reflecting the impact of the more distinct hydrophobic/hydrophilic surface of these generalized nanopores. The replacement of charged residues (in HL) by Trp residues in Gβ results only in a small extra effect on pore tilt angles, contrary to the effect that Trp residues seem to have on the tilt experienced by α-helical nanopores in lipid bilayers. This may be due to the reduced representation of Trp in the current force field, meaning that the CG side-chain particles have similar Lennard-Jones interactions to the lipid headgroups when compared with the charged residues in

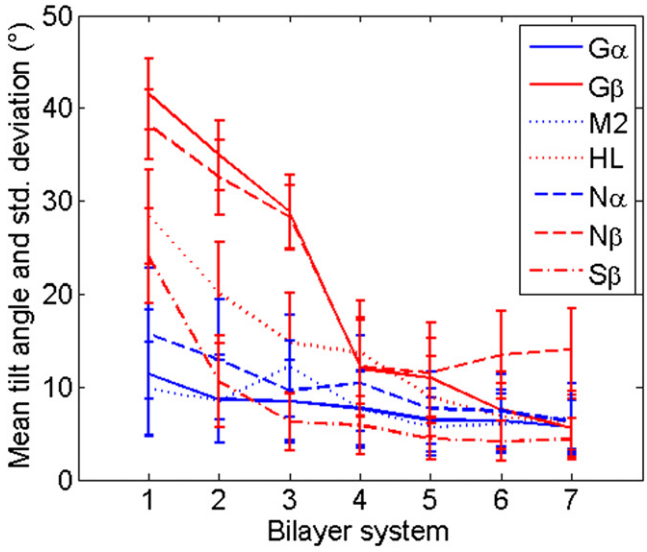

FIGURE 6 Mean tilt angles with SDs versus bilayer thickness of the nanopore-lipid bilayer systems studied. The bilayer thickness (defined as the distance between the phosphate particles of opposing monolayers, d_{PP}) is implicitly shown as a function of the lipid bilayer system, defined as follows: 1 = CG2-PC, 2 = CG2-PC + CG3-PC, 3 = CG3-PC, 4 = CG3-PC + CG4-PC, 5 = CG4-PC, 6 = CG4-PC + CG5-PC, 7 = CG5-PC.

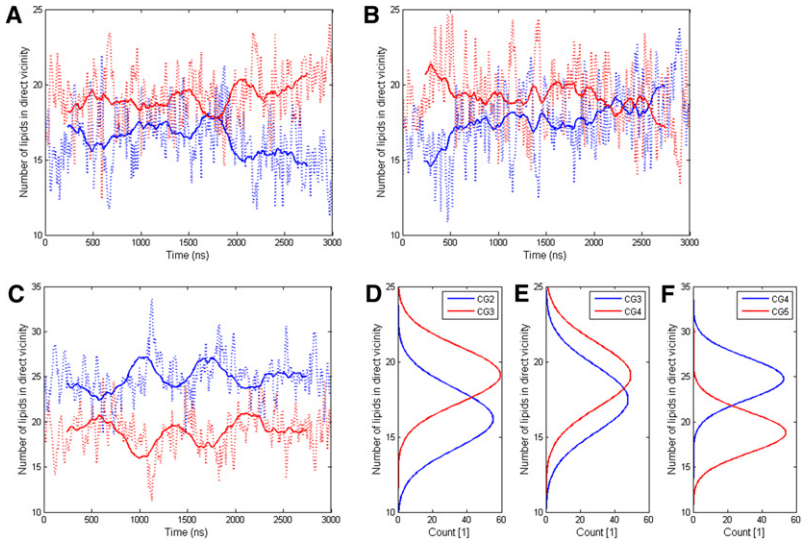

FIGURE 7 Number of lipids in direct vicinity of the Gα nanopore over time in the CG2-PC+CG3-PC (*A* and *D*), CG3-PC+CG4-PC (*B* and *E*), and CG4-PC+CG5-PC (*C* and *F*) bilayer systems. Plots *D–F* display the histograms for the number of lipids of the respective lipid types in the first shell around the nanopore. Each plot shows the average number of lipids of both types in the vicinity of the nanopore for 3 μs CG-MD simulations. The solid lines represent a moving average for a window size of 50 ns.

HL. However, in the M2-to-Gα substitution, Thr and Ser residues are replaced. These have a much stronger interaction with the lipid headgroups, and thus their removal alters the tilt to a greater extent. The complete removal of Trp residues seems to reduce the stability of the nanopores, causing a greater tilt within the bilayer (see Fig. 6). This is noticeable for all Nα systems and the Nβ systems with thicker bilayers, as the effect may be masked for Nβ systems in narrower bilayers by the extreme nanopore tilting (~40°) and also by the larger error bars observed for narrower bilayers.

Overall, this behavior is consistent with the behavior of the simple model proteins in earlier studies (9,37). Furthermore, for isolated α-helices, a correlation between the system composition (i.e., the level of hydrophobic mismatch) and the degree of lipid bilayer-induced nanopore tilting has been suggested in AT-MD studies (4,57) and solid-state NMR experiments (54). However, one must remember that a recent study (6) indicated that earlier experimental studies may have underestimated helix tilt angle, leading to an apparent disagreement with experiment. Similarly, one should be careful when comparing our findings with the results of recent spectroscopic studies of β-barrel proteins (58,59). However, in general it would seem that current experimental studies suggest a greater possible degree of tilting than was assumed previously.

Distribution of lipid types in mixed-lipid bilayers

In mixed lipid bilayers, a large hydrophobic mismatch between lipid bilayer and nanopores suggests the possibility of a lipid sorting mechanism (60). In the case of local bilayer stretching (i.e., the average hydrophobic length of the lipid bilayer is less than that of the nanopore), the longer lipids are expected to accumulate in close proximity to the nanopore, locally reducing the hydrophobic mismatch. In contrast, in the case of local bilayer compression (the hydrophobic length of the lipid bilayer is longer than that of the nanopore), the shorter lipids are expected to accumulate around the nanopore, resulting in local bilayer thinning.

To study the distribution of lipids in a mixed-lipid bilayer, 3 μs CG-MD simulations of the three mixed-lipid systems were run and the cumulative radial distribution functions for both lipid types around the Gα nanopore were calculated for each frame. The radial distribution density around the nanopore was used to calculate an approximate radius for the first shell of lipids (a single layer of lipids; cf. Supporting Material) around the nanopore. Next, the number of lipids of each lipid type within that shell was calculated for each frame of the simulation and displayed as a function of time (Fig. 7).

For the Gα nanopore in a CG2-PC+CG3-PC bilayer (Fig. 7), a system where the lipid bilayer is stretched, it can be seen that the longer lipid type (CG3-PC) accumulates around the nanopore over time. The opposite happens for the Gα nanopore-CG4-PC+CG5-PC lipid bilayer system (Fig. 7, *E* and *F*), as now the lipid bilayer is compressed in proximity to the nanopore and therefore the shorter lipid type (CG4-PC) accumulates around the nanopore over time. For the Gα nanopore in a CG3-PC+CG4-PC lipid bilayer (Fig. 7, *C* and *D*), both lipid types share the environment around the nanopore to an approximately equal extent. This indicates that hydrophobic mismatch may be a driving force for lipid sorting in mixed-lipid bilayers.

In an additional analysis, we demonstrated that every lipid appeared in the first shell of lipids around the nanopore at some stage during a simulation of 3 μs duration (data not shown), thus demonstrating that the lipids are free to exchange positions on the simulation timescales accessed. However, some lipid molecules seemed to be more often in the first shell than others, reflecting the fact that the simulation time was short and they started closer to the nanopores. The important finding was that lipids did not remain bound to the nanopore throughout the simulation, which would otherwise have biased our results.

DISCUSSION

In this study, we have shown that there is a reciprocal interplay in the interactions between nanopores and lipid bilayers. This therefore extends previous systematic studies that either examined simplified nanopore/protein models (9,10,37,61) or focused on single α-helices (4). In this work we studied three interactions: nanopore-induced local bilayer perturbations, bilayer-induced nanopore tilting, and local (re)distribution of lipid types in mixed-lipid bilayers.

In terms of nanopore-induced lipid bilayer perturbations, our results suggest that the length of a nanopore, in addition to the hydrophobic mismatch, steers lipid bilayer perturbations, supporting a previously developed hypothesis (52). The first derivatives of the radial bilayer thickness profiles clarify that the local bilayer perturbations, caused by the inserted nanopore, show to a first approximation an exponential behavior and decay in a distance of 30–60 Å from the nanopore COM. These findings are consistent with the behavior of rather more abstract model proteins/nanopores in previous studies (9,10,25,37).

The local lipid bilayer perturbations caused by inserted nanopores suggest a possible method for lipid bilayer-induced protein sorting, as proteins experiencing a strong hydrophobic mismatch are more likely to associate to reduce the overall local perturbations of the lipid bilayer, minimizing the free energy of the system. A preliminary test of this hypothesis on a set of simulations of multiple Gα nanopores in a 1600 CG5-PC bilayer (cf. Supporting Material, Fig. S10) suggested that association of the nanopores to give aggregates in the plane of the bilayer occurred over the course of a 500 ns CG-MD simulation. Note that because of the nature of CG-MD (i.e., smoother particle-particle interaction potentials), the kinetics are increased, so that 1 ns in CD-MD simulation time may represent ~5–7 ns in AT-MD time (45), and thus, 500 ns of CG-MD may be equivalent to ~3 μs simulation time in AT-MD. Similar behavior was observed in CG-MD simulations of oligomerization of rhodopsin (16).

The results for lipid bilayer-induced nanopore tilt angles showed a correlation between a smaller lipid bilayer thickness (causing larger hydrophobic mismatch) and a larger tilt angle, as has been observed in a number of other studies, both experimental and computational (4,9,10,14,25,37,54,62). Also, in the case of larger hydrophobic mismatches, the simulated tilt angle distributions seemed to broaden, indicating a larger fluctuation of nanopore tilt angles. Furthermore, nanopore size as well as key residues (e.g., Trp) seemed to influence the degree of the lipid-bilayer induced nanopore tilt. It was found that neither the hydrophobic length of the nanopore (as a measure for the hydrophobic mismatch) nor the nanopore dimensions solely correlate with the simulated tilt angles. Thus, to fully understand interactions with a bilayer, a model of the nanopore that includes specific residue types is needed.

Finally, lipid distribution in mixed-lipid systems was studied. In the case of local bilayer stretching, the longer lipids accumulated as expected in close proximity to the nanopore, reducing the amount of hydrophobic mismatch. Likewise, in the case of local bilayer compression, the shorter lipids accumulated around the nanopore. These results seem to confirm the hypothesis that in mixed-type lipid bilayers, a large hydrophobic mismatch between the lipid bilayer and the nanopore drives a lipid sorting mechanism (60,61).

There are a number of technical limitations to the studies presented here. It should be noted that an elastic network was used to model the secondary and tertiary structures of the proteins. Thus, the differences in interactions noted between α-helical and β-barrel pores relate mainly to differences in the outer surfaces of the TM domains of the two classes of nanopore, and not to possible differences in rigidity between the two types of structure. Furthermore, although the CG force-field parameters have been tested on a number of peptides and proteins against various experimental data (26,48), there have been further developments in CG force fields that could be explored (31). Another limitation is that, although the lipid tail lengths were varied, only a single lipid headgroup species (PC) was used. This could be explored further in the future, especially given that CG-MD was recently shown to reproduce well the properties of different lipid species (30).

This study could be extended in a number of future directions. One would be to use the final configurations from the CG simulations as the starting point for atomistic simulations. This would enable investigators to probe the bilayer/nanopore interactions in more detail and to overcome the possible limitations of the CG force field in terms of, e.g., aromatic/cation interactions in side-chain/lipid headgroup interactions. Another possibility is to use the generalized nanopore models as design tools for probing further interactions with different lipid bilayer systems, both computationally and experimentally.

SUPPORTING MATERIAL

Eleven figures and two tables are available at http://www.biophysj.org/biophysj/supplemental/S0006-3495(09)00578-5.

J.W.K. and T.C. recognize the financial assistance of the Engineering and Physical Sciences Research Council and the Biotechnology and Biological Sciences Research Council, respectively. Research in M.S.P.S.'s laboratory is supported by the Biotechnology and Biological Sciences Research Council, Engineering and Physical Sciences Research Council, Medical Research Council, and the Wellcome Trust. The authors declare no conflict of interest.

REFERENCES

1. Lee, A. G. 2005. How lipids and proteins interact in a membrane: a molecular approach. *Mol. Biosyst.* 1:203–212.
2. Lindahl, E., and M. S. P. Sansom. 2008. Membrane proteins: molecular dynamics simulations. *Curr. Opin. Struct. Biol.* 18:425–431.
3. Killian, J. A., and T. K. M. Nyholm. 2006. Peptides in lipid bilayers: the power of simple models. *Curr. Opin. Struct. Biol.* 16:473–479.

4. Kandasamy, S. K., and R. G. Larson. 2006. Molecular dynamics simulations of model trans-membrane peptides in lipid bilayers: a systematic investigation of hydrophobic mismatch. *Biophys. J.* 90:2326–2343.
5. Nyholm, T. K. M., S. Ozdirekcan, and J. A. Killian. 2007. How protein transmembrane segments sense the lipid environment. *Biochemistry.* 46:1457–1465.
6. Ozdirekcan, S., C. Etchebest, J. A. Killian, and P. F. J. Fuchs. 2007. On the orientation of a designed transmembrane peptide: toward the right tilt angle? *J. Am. Chem. Soc.* 129:15174–15181.
7. Lopez, C. F., S. O. Nielsen, P. B. Moore, and M. L. Klein. 2004. Understanding nature's design for a nanosyringe. *Proc. Natl. Acad. Sci. USA.* 101:4431–4434.
8. Lopez, C. F., S. O. Nielsen, B. Ensing, P. B. Moore, and M. L. Klein. 2005. Structure and dynamics of model pore insertion into a membrane. *Biophys. J.* 88:3083–3094.
9. Venturoli, M., B. Smit, and M. M. Sperotto. 2005. Simulation studies of protein-induced bilayer deformations, and lipid-induced protein tilting, on a mesoscopic model for lipid bilayers with embedded proteins. *Biophys. J.* 88:1778–1798.
10. Schmidt, U., G. Guigas, and M. Weiss. 2008. Cluster formation of transmembrane proteins due to hydrophobic matching. *Phys. Rev. Lett.* 101:128104.
11. Bayley, H., and P. S. Cremer. 2001. Stochastic sensors inspired by biology. *Nature.* 413:226–230.
12. Marrink, S. J., A. H. de Vries, and A. E. Mark. 2004. Coarse grained model for semiquantitative lipid simulations. *J. Phys. Chem. B.* 108:750–760.
13. Gil, T., J. H. Ipsen, O. G. Mouritsen, M. C. Sabra, M. M. Sperotto, et al. 1998. Theoretical analysis of protein organization in lipid membranes. *Biochim. Biophys. Acta.* 1376:245–266.
14. Sperotto, M. M., S. May, and A. Baumgaertner. 2006. Modelling of proteins in membranes. *Chem. Phys. Lipids.* 141:2–29.
15. Venturoli, M., M. M. Sperotto, M. Kranenburg, and B. Smit. 2006. Mesoscopic models of biological membranes. *Phys. Rep.* 437:1–54.
16. Periole, X., T. Huber, S. J. Marrink, and T. P. Sakmar. 2007. G protein-coupled receptors self-assemble in dynamics simulations of model bilayers. *J. Am. Chem. Soc.* 129:10126–10132.
17. Baumgärtner, A. 1996. Insertion and hairpin formation of membrane proteins: a Monte Carlo study. *Biophys. J.* 71:1248–1255.
18. Shelley, J. C., M. Y. Shelley, R. C. Reeder, S. Bandyopadhyay, and M. L. Klein. 2001. A coarse grain model for phospholipid simulations. *J. Phys. Chem. B.* 105:4464–4470.
19. Murtola, T., E. Falck, M. Patra, M. Karttunen, and I. Vattulainen. 2004. Coarse-grained model for phospholipid/cholesterol bilayer. *J. Chem. Phys.* 121:9156–9165.
20. Nielsen, S. O., C. F. Lopez, G. Srinivas, and M. L. Klein. 2004. Coarse grain models and the computer simulation of soft materials. *J. Phys. Condens. Matter.* 16:R481–R512.
21. Stevens, M. J. 2004. Coarse-grained simulations of lipid bilayers. *J. Chem. Phys.* 121:11942–11948.
22. Izvekov, S., and G. A. Voth. 2005. A multiscale coarse-graining method for biomolecular systems. *J. Phys. Chem. B.* 109:2469–2473.
23. Shi, Q., S. Izvekov, and G. A. Voth. 2006. Mixed atomistic and coarse-grained molecular dynamics: simulation of a membrane bound ion channel. *J. Phys. Chem. B.* 110:15045–15048.
24. Shih, A. Y., A. Arkhipov, P. L. Freddolino, and K. Schulten. 2006. Coarse grained protein-lipid model with application to lipoprotein particles. *J. Phys. Chem. B.* 110:3674–3684.
25. Smeijers, A. F., K. Pieterse, A. J. Markvoort, and P. A. J. Hilbers. 2006. Coarse-grained transmembrane proteins: Hydrophobic matching, aggregation, and their effect on fusion. *J. Phys. Chem. B.* 110:13614–13623.
26. Bond, P. J., J. Holyoake, A. Ivetac, S. Khalid, and M. S. P. Sansom. 2007. Coarse-grained molecular dynamics simulations of membrane proteins and peptides. *J. Struct. Biol.* 157:593–605.
27. Marrink, S. J., J. Risselada, S. Yefimov, D. P. Tieleman, and A. H. de Vries. 2007. The MARTINI forcefield: coarse grained model for biomolecular simulations. *J. Phys. Chem. B.* 111:7812–7824.
28. May, E. R., A. Narang, and D. I. Kopelevich. 2007. Role of molecular tilt in thermal fluctuations of lipid membranes. *Phys. Rev. E Stat. Nonlin. Soft Matter Phys.* 76:021913.
29. Orsi, M., D. Y. Haubertin, W. E. Sanderson, and J. W. Essex. 2008. A quantitative coarse-grain model for lipid bilayers. *J. Phys. Chem. B.* 112:802–815.
30. May, E. R., D. I. Kopelevich, and A. Narang. 2008. Coarse-grained molecular dynamics simulations of phase transitions in mixed lipid systems containing LPA, DOPA, and DOPE lipids. *Biophys. J.* 94:878–890.
31. Monticelli, L., S. K. Kandasamy, X. Periole, R. G. Larson, D. P. Tieleman, et al. 2008. The MARTINI coarse grained force field: extension to proteins. *J. Chem. Theory Comput.* 4:819–834.
32. Yefimov, S., E. van der Giessen, P. R. Onck, and S. J. Marrink. 2008. Mechanosensitive membrane channels in action. *Biophys. J.* 94:2994–3002.
33. Killian, J. A. 1998. Hydrophobic mismatch between proteins and lipids in membranes. *Biochim. Biophys. Acta.* 1376:401–416.
34. Andersen, O. S., and R. E. Koeppe. 2007. Bilayer thickness and membrane protein function: an energetic perspective. *Annu. Rev. Biophys. Biomol. Struct.* 36:107–130.
35. de Planque, M. R. R., E. Goormaghtigh, D. V. Greathouse, R. E. Koeppe, J. A. W. Kruijtzer, et al. 2001. Sensitivity of single membrane-spanning α-helical peptides to hydrophobic mismatch with a lipid bilayer: effects on backbone structure, orientation, and extent of membrane incorporation. *Biochemistry.* 40:5000–5010.
36. Popot, J. L., and D. M. Engelman. 2000. Helical membrane protein folding, stability, and evolution. *Annu. Rev. Biochem.* 69:881–922.
37. Nielsen, S. O., B. Ensing, V. Ortiz, P. B. Moore, and M. L. Klein. 2005. Lipid bilayer perturbations around a transmembrane nanotube: a coarse grain molecular dynamics study. *Biophys. J.* 88:3822–3828.
38. Opella, S. J., F. M. Marassi, J. J. Gesell, A. P. Valente, Y. Kim, et al. 1999. Structures of the M2 channel-lining segments from nicotinic acetylcholine and NMDA receptors by NMR spectroscopy. *Nat. Struct. Biol.* 6:374–379.
39. Saiz, L., S. Bandyopadhyay, and M. L. Klein. 2004. Effect of the pore region of a transmembrane ion channel on the physical properties of a simple membrane. *J. Phys. Chem. B.* 108:2608–2613.
40. Song, L., M. R. Hobaugh, C. Shustak, S. Cheley, H. Bayley, et al. 1996. Structure of staphylococcal α-hemolysin, a heptameric transmembrane pore. *Science.* 274:1859–1866.
41. Yau, W. M., W. C. Wimley, K. Gawrisch, and S. H. White. 1998. The preference of tryptophan for membrane interfaces. *Biochemistry.* 37:14713–14718.
42. de Planque, M. R. R., J. A. W. Kruijtzer, R. M. J. Liskamp, D. Marsh, D. V. Greathouse, et al. 1999. Different membrane anchoring positions of tryptophan and lysine in synthetic transmembrane α-helical peptides. *J. Biol. Chem.* 274:20839–20846.
43. Lear, J. D., Z. R. Wasserman, and W. F. DeGrado. 1988. Synthetic amphiphilic peptide models for protein ion channels. *Science.* 240:1177–1181.
44. Marrink, S. J., E. Lindahl, O. Edholm, and A. E. Mark. 2001. Simulation of the spontaneous aggregation of phospholipids into bilayers. *J. Am. Chem. Soc.* 123:8638–8639.
45. Bond, P. J., and M. S. P. Sansom. 2006. Insertion and assembly of membrane proteins via simulation. *J. Am. Chem. Soc.* 128:2697–2704.
46. van der Spoel, D., E. Lindahl, B. Hess, G. Groenhof, A. E. Mark, et al. 2005. GROMACS: fast, flexible, and free. *J. Comput. Chem.* 26:1701–1718.
47. Bond, P. J., and M. S. P. Sansom. 2007. Bilayer deformation by the Kv channel voltage sensor domain revealed by self-assembly simulations. *Proc. Natl. Acad. Sci. USA.* 104:2631–2636.

48. Bond, P. J., C. L. Wee, and M. S. P. Sansom. 2008. Coarse-grained molecular dynamics simulations of the energetics of helix insertion into a lipid bilayer. *Biochemistry*. 47:11321–11331.

49. Berendsen, H. J. C., J. P. M. Postma, W. F. van Gunsteren, A. DiNola, and J. R. Haak. 1984. Molecular dynamics with coupling to an external bath. *J. Chem. Phys*. 81:3684–3690.

50. Humphrey, W., A. Dalke, and K. Schulten. 1996. VMD—Visual Molecular Dynamics. *J. Mol. Graph*. 14:33–38.

51. Tieleman, D. P., and H. J. C. Berendsen. 1996. Molecular dynamics simulations of a fully hydrated dipalmitoylphosphatidycholine bilayer with different macroscopic boundary conditions and parameters. *J. Chem. Phys*. 105:4871–4880.

52. Ridder, A. N., R. E. Spelbrink, J. A. Demmers, D. T. Rijkers, R. M. Liskamp, et al. 2004. Photo-crosslinking analysis of preferential interactions between a transmembrane peptide and matching lipids. *Biochemistry*. 43:4482–4489.

53. van der Wel, P. C. A., E. Strandberg, J. A. Killian, and R. E. Koeppe. 2002. Geometry and intrinsic tilt of a tryptophan-anchored transmembrane α-helix determined by ^{2}H NMR. *Biophys. J*. 83:1479–1488.

54. Strandberg, E., S. Özdirekcan, D. T. S. Rijkers, P. C. A. van der Wel, R. E. Koeppe, II, et al. 2004. Tilt angles of transmembrane model peptides in oriented and non-oriented lipid bilayers as determined by ^{2}H solid-state NMR. *Biophys. J*. 86:3709–3721.

55. Sengupta, D., L. Meinhold, D. Langosch, G. M. Ullmann, and J. C. Smith. 2005. Understanding the energetics of helical peptide orientation in membranes. *Proteins*. 58:913–922.

56. Ulmschneider, M. B., M. S. P. Sansom, and A. Di Nola. 2006. Evaluating tilt angles of membrane-associated helices: comparison of computational and NMR techniques. *Biophys. J*. 90:1650–1660.

57. Petrache, H. I., D. M. Zuckerman, J. N. Sachs, J. A. Killian, R. E. Koeppe, et al. 2002. Hydrophobic matching mechanism investigated by molecular dynamics simulations. *Langmuir*. 18:1340–1351.

58. Anbazhagan, V., N. Vijay, J. H. Kleinschmidt, and D. Marsh. 2008. Protein-lipid interactions with Fusobacterium nucleatum major outer membrane protein FomA: spin-label EPR and polarized infrared spectroscopy. *Biochemistry*. 47:8414–8423.

59. Anbazhagan, V., J. Qu, J. H. Kleinschmidt, and D. Marsh. 2008. Incorporation of outer membrane protein OmpG in lipid membranes: protein-lipid interactions and β-barrel orientation. *Biochemistry*. 47:6189–6198.

60. Dumas, F., M. M. Sperotto, M. C. Lebrun, J. F. Tocanne, and O. G. Mouritsen. 1997. Molecular sorting of lipids by bacteriorhodopsin in dilauroylphophatidylcholine/distearoylphosphatidylcholine lipid bilayers. *Biophys. J*. 73:1940–1953.

61. Nielsen, S. O., C. F. Lopez, I. Ivanov, P. B. Moore, J. C. Shelley, et al. 2004. Transmembrane peptide-induced lipid sorting and mechanism of L-α-to-inverted phase transition using coarse-grain molecular dynamics. *Biophys. J*. 87:2107–2115.

62. Koehorst, R. B. M., R. B. Spruijt, F. J. Vergeldt, and M. A. Hemminga. 2004. Lipid bilayer topology of the transmembrane α-helix of M13 major coat protein and bilayer polarity profile by site-directed fluorescence spectroscopy. *Biophys. J*. 87:1445–1455.